Molecular Crystals and Liquid Crystals

ISSN: 1542-1406 (Print) 1563-5287 (Online) Journal homepage: http://www.tandfonline.com/loi/gmcl20

Improved modal observer for modal SSDI-Max

E. Babesse, S. Belkhiat, A. Cherif, M. Meddad, A. Eddiai & Y. Boughaleb

To cite this article: E. Babesse, S. Belkhiat, A. Cherif, M. Meddad, A. Eddiai & Y. Boughaleb (2016) Improved modal observer for modal SSDI-Max, Molecular Crystals and Liquid Crystals, 628:1, 145-161, DOI: 10.1080/15421406.2015.1137118

To link to this article: http://dx.doi.org/10.1080/15421406.2015.1137118

Published online: 13 May 2016.

MOL. CRYST. LIQ. CRYST.
2016, VOL. 628, 145–161
http://dx.doi.org/10.1080/15421406.2015.1137118

Taylor & Francis
Taylor & Francis Group

Improved modal observer for modal SSDI-Max

E. Babesse[a], S. Belkhiat[a], A. Cherif[b], M. Meddad[b], A. Eddiai[c], and Y. Boughaleb[d]

[a]DAC HR Laboratory, University of Sétif, Algeria; [b]DAC HR Laboratory Sétif, University Mohamed el Bachir el Ibrahimi BBA, Algeria; [c]Laboratoire de physique de la matière condensée, Faculté des Sciences Ben M'sik, Université Hassan II de Casablanca, Morocco; [d]Département de Physique, Faculté des Sciences, Laboratoire de Physique de la Matière Condensée (LPMC), 24000 El Jadida, Morocco

ABSTRACT

The objective of this paper is to improve a semi-active control of structural vibrations, which is Synchronised Switch Damping on Inductor Maximum. The improvement is attained by adding a system to estimate the structure modal displacement. A model of smart structure shunted to resonant circuit is used and tested with Matlab™ environment and the performance of the new strategy based on Lenear Quadratic Guaussian and Neuro-Fuzzy observer are presented and compared with that one based on Proportional Integral Derivative observer. Results shows the new technique effectiveness when conventional one reaches its limits in the wide bande frequency case.

KEYWORDS

Semi-passive technique; Modal strategy; Modal observer; Vibration damping; Piezoelectric transducer.

1. Introduction

In the recent years, vibrations damping is a technological area interesting several researchers whereas it concerns many industrial and military applications. Within this framework, many methods of vibrations damping via piezoelectric materials were proposed. These methods can be classified in three classes according to the external energy and the complexity of the used control chain. There are three types: passive control, active control and semi-active control.

The passive control, beeing the earliest, consists in connecting the piezoelectric element to a passive circuit (R, RL) (R. L. Forward, 1979; N. W. Hagood and A. Von Flotow, 1991). This type of control has the advantage of requiring neither energy to work as well as the great simplicity of implementation. Nevertheless, the method is very sensitive to the environmental variations and drives thus to damp only one mode of vibration.

The active control is a technique which aims at imposing a force or a displacement in certain points of the system to be controlled as a function, especially, of the measured state or the history of this one (C. H. Park and D. J. Inman, 2003; A. J. Fleming and S. O. R. Moheimani, 2003). Although very effective, these approaches imply several disadvantages including the use of complexe chain composed of a calculating unit, sensors and transducers, control strategy and voltage generators and/or amplifiers to supply the actuators. The ineffectiveness of the passive technics and the complexity of the active ones were originate of the semi-active (called also semi-passive) control methods development. The semi-passive and semi-active methods can be distinguished by the use of the small amount external energy. This energy

CONTACT E. Babesse babessew@yahoo.fr
Color versions of one or more of the figures in the article can be found online at www.tandfonline.com/gmcl.

is only used for power-up the control system. Otherwise, there is a semi-active control (A. Chérif et al., 2013).The semi-active strategy is an innovative alternative to active control. It is a technique which carries out a nonlinear treatment of the voltage generated by the piezoelectric elements, without need a great quantity of external energy which can be self-supplied (M. Lallart, 2010.).

The first semi-active methods installation consist in commutating the piezoelectric element from an open circuit state to a short-circuit state called later "Synchronized Switch Damping Short-circuit (SSDS)" (C. Richard et al.,1999). The piezoelectric element is short-circuited at each extreme of strain (or of displacement).This technique was improved by the addition of an inductance in the circuit in order to increase the electric charge present in the piezoelectric element. This strategy named "Synchronized Switch Damping on Inductor" (SSDI) has been carried out in (C. Richard et al., 2000). It is almost identical to that of the SSDS, except that instead of forcing the voltage to zero extreme at each displacement, this is the voltage which is reversed and can increased by connecting the piezoelectric elements to a continuous voltage source (SSDV) (A. Badel et al., 2006). This control makes it possible to improve the performances of damping but the method requires an external source of energy. However, the need of external energy source is rather a disadvantage of the method. The SSDI development aims so to enhancing the performance of the SSDV technic, such as carried out in (B. Mokrani et al., 2011). The enhancement was achieved by adding a negative capacitance to the resonant circuit that dissipates the energy converted by the piezoelectric transducer. Afterwards, the methods have been improved in order to control the systems subject to broadband excitations. Among these methods, there is that one baptized modal SSDI-Max. This modal technic has been developed in the first time by (S. Harari et al., 2009) and has been used in many works such as in (A. Chérif et al., 2013) and (E. Babesse et al., 2013). It consists in combining the advantages of the both active and the semi-active methods. For that, a modal model has been proposed and a modal observer has been developed to rebuild the modal coordinates of the system within,the control can be targeted on the most energetic modes.The modal strategy performances were substantially related to the performances of the observer used whereas, inversions were located in the extreme of the modal displacements given by this observer.

A performances analysis of modal SSDI-Max using an enhanced LQG + Neuro-Fuzzy observer is presented in this work. The results were compared with that one obtained by the LQG + PID observer carried out in the precedent work (A. Chérif et al.,2012). The object of the work aims to improve the modal displacement image given by the observer and to maximize the self-generated voltage whereas the method has been used to improve the performances of the piezo transformer (A. Chérif et al., 2013). Simulations are performed on a model representative of a clamped plate. The results are given in the cases of multi-sinusoidal, pulse, and white noise excitations.

2. Smart structure modeling

The electromechanical behavior of an intelligent structure (instrumented of piezoelectric elements) is given by the following equations:

$$M\ddot{\delta} + C\dot{\delta} + K^E q = -\alpha V + \beta F, \tag{1}$$

$$I = \alpha^t \dot{\delta} - C_0 \dot{V}, \tag{2}$$

With δ is the vector of displacement, M, C and K^E are respectively the matrices of mass, damping and rigidity when the piezoelectric patches are in short-circuit. α is the electromechanical matrix of coupling, V is a voltage vector of the piezoelectric patch, I is the electrical current vector, and C_0 is the diagonal matrix of patches capacitances. F is the force applied to the system.

Carrying out the change of variable according to:

$$\delta = \varphi q, \tag{3}$$

Where φ is the mode matrix of the structure limited to n modes and q is the vector of modal displacement of the structure. Equations (1) and (2) become:

$$M\ddot{q} + C\dot{q} + K^E q = -\theta V + \beta F, \tag{4}$$

$$I = \theta^t \dot{q} - C_0 \dot{V}, \tag{5}$$

With $\theta = \varphi^t . \alpha$, is the modal matrix of electromechanical coupling of size $[n, i]$. M, C, K^E are respectively the modal matrices of the mass, damping and rigidity.

The equation (2) is standardized in order to have:

$$M = I_d\,;\; C = 2\,diag\,(\xi)\,diag\,(\omega^D);\; K^E = diag\left(\left(\omega^E\right)^2\right),$$

With ξ is the vector of modal damping, ω^E is the vector of the frequency in short-circuit and ω^D the vector of frequency in open circuit.

While separating the voltages of the transducers and the sensors, I_s and V_s respectively, and when the sensor voltage is supervised by a voltage amplifier (whose intensity of the sensor is null). Equations (4) and (5) become:

$$M\ddot{q} + C\dot{q} + K^E q = -\theta_a V_a - \theta_s V_s + \beta F, \tag{6}$$

$$\theta_s^t q - C_{0s} V_s = 0, \tag{7}$$

By substitution of (7) in (6) one found:

$$M\ddot{q} + C\dot{q} + \left(K^E + \theta_s\,(C_{0s})^{-1}\,\theta_s^t\right) q = -\theta_a V_a + \beta F, \tag{8}$$

The system of linear equations (7) and (8) can be written in the form:

$$\begin{cases} \dot{x} = A x + Bu, \\ y = C x, \end{cases} \qquad x = \begin{bmatrix} q \\ \dot{q} \end{bmatrix} \tag{9}$$

$U = \begin{bmatrix} F & V_a \end{bmatrix}$,is the control vector;$U = \begin{bmatrix} q & \dot{q} \end{bmatrix}$, V_s is the output vector, A, B, C are the state matrices:

$$A = \begin{bmatrix} 0 & I_d \\ -M^{-1}\left(K^E + \theta_s\, C_{0s}^{-1}\,\theta_s^t\right) & -M^{-1} C \end{bmatrix},$$

$$B = \begin{bmatrix} 0 \\ +M^{-1}\beta \quad -M^{-1}\theta_a \end{bmatrix},\quad C = \begin{pmatrix} I_d & 0 \\ 0 & I_d \\ C_{0s}^{-1}\,\theta_s^t & 0 \end{pmatrix},$$

V_a is calculated by the following relation:

$$V_a = C_{0a}^{-1}\;\theta_a^t\, q,$$

C_{0a} and C_{0s} are the capacity matrices of transducers and sensors respectively.

The structure used in the following simulations is that one carried out in the references (D. Guyomar et al., 2008) and (S. Harari et al., 2009).

3. Modal SSDI-Max control

Modal SSDI-Max control based on SSDI strategy was associated to a modal observer which provides the disired modes. Recalling in the following sections the principle of each method.

3.1 SSDI control

The SSDI control (Synchronized Switch Damping on Inductor) consists in using an electronic switch which was controlled during brief moments in a synchronous way with the vibration. When the voltage of the piezoelectric elements is extreme, the switch connects the piezoelectric elements to an electric circuit composed of an inductance driving to reverse the voltage. This inversion was based on the capacity C_0 of the piezoelectric elements and the inductance L which form an oscillating electric circuit. The inversion induces a mechanical force of sign opposed at the speed, thus obtaining the desired damping (A. Chérif et al., 2012), (S. Harari et al.,2009) and (S. Harari et al.,2009).

3.2 SSDI-Max control

The SSDI-Max technique is an improvement of SSDI technique where the commutation occurred in the local maxima. It consists in immediately delaying the moment spent to the extreme of following voltage after the extreme of targeted modal coordinate. This process is illustrated in the Figure 1. The algorithm of the strategy is summarized in (A.Chérif et al., 2012) as fellows:

When a maximum of modal displacement appears, the window of time limitation starts. Thus the signs of the voltage V_a and its derivative are considered during the window:

- If the voltage is positive and the derivative is negative, the switch trigger is immediate.
- If the voltage is positive and the derivative is positive, the system waits for the next maximum voltage. This delay is nevertheless limited by the window of time.
- If no switching occurred and the end of the time window is reached, the switching is triggered.

This algorithm is antisymmetric if a minimum modal displacement is reached.

3.3 Modal strategy

The strategy of control SSDI/SSDI-Max is adequately used for single frequency excitation signals. In the broadband excitation, the method reaches its limits. These ones are due to the many inversions of voltage having many small amplitudes. The significant number of inversions in the same time does not make it possible consequently to maximize the transducer voltage and to target certain modes control of the structure. Otherwise, the action localization surrounding energy modes contributes to improve the effectiveness of control.

Thus in order to avoid these disadvantages, modal strategy was developed (S. Harari et al., 2009). So as to target certain modes, the suggested method consists in reversing the transducer voltage when the displacement of the targeted mode is extreme. The Figure 2 presents the transducer voltage V_a related to modal displacement qi (S. Harari et al., 2009).

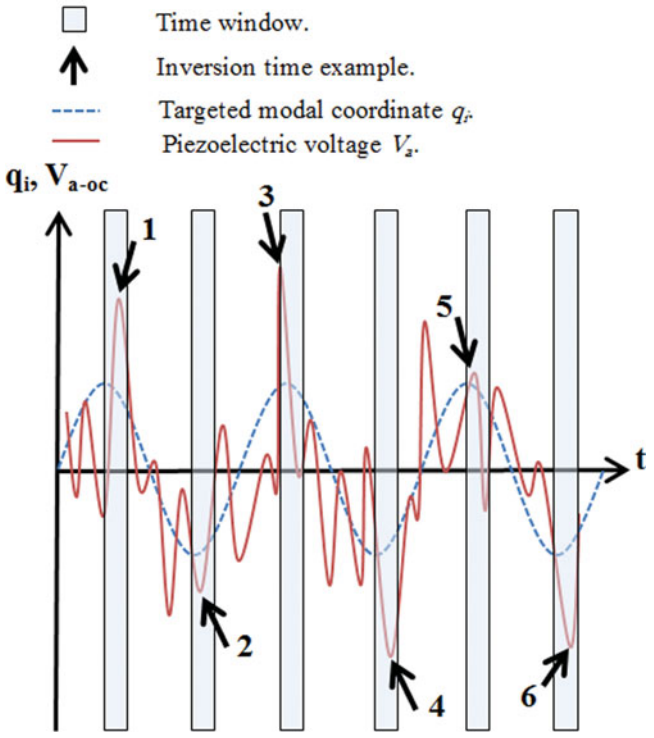

Figure 1. The SSDI-Max strategy illustration: the definition of the switching moment according to the targeted modal coordinate and the piezoelectric transducer voltage in open circuit and the authorized maximum time.

The inversion of the voltage, when selected modal displacement is extreme, is possible only if the modal displacement is available, but this latter is not accessible directly via measurements. There is therefore necessity to estimate it. In this way, a modal observer is used (S. Harari et al., 2009).

Figure 3 shows the SSDI/SSDI-Max modal control architecture. As it is shown in the diagram (Figure 3), the observer role is decisive in this type of strategy, whereas the moments of commutation, which define the quality of damping, are largely dependent of this observer.

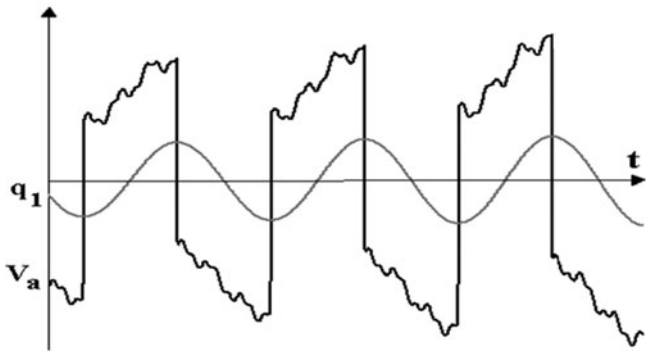

Figure 2. Wave form of the voltage, where V_a is the piezoelectric transducer voltage and q_1 is the corresponding first modal displacement.

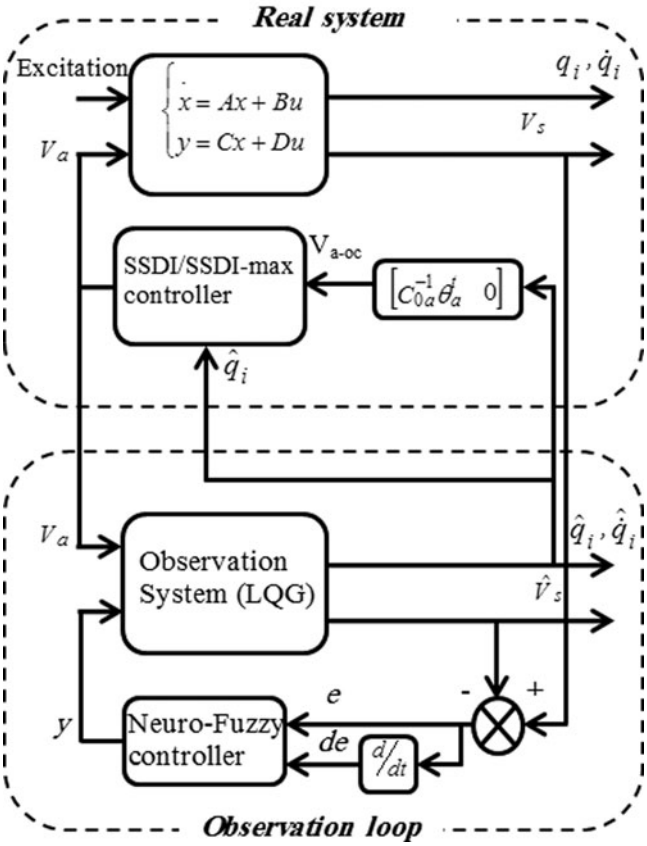

Figure 3. Modal SSDI/SSDI- Max control architecture.

3.4 Modal observer

The modal observer used in this work consists in deriving from the measurement voltages V_s the modal coordinate q_i to trigger the commutation device. The loop of observation will estimate in the same time the state space vector and the sensors voltages; therefore the equation of control in closed loop is expressed by,

$$\dot{\hat{x}} = A\hat{x} + BV_a - L\left(V_s - \hat{V}_s\right),$$

Gain matrix L must be selected so that the error on the state will be stable and disappears quickly with a great dynamic; faster than the structure itself. To calculate this matrix, the method LQG was chosen (D. Luenberger, 1971). Otherwise, LQG technique does not guarantee the good properties.

In order to ensure an adequate stability of the system and to improve the global performances, the solution consisted in adding an external loop implementing a regulator PID (A. Chérif et al., 2012).

The implementations of estimator LQG and regulator PID are detailed in the references (A. Chérif et al., 2012; T. Richard, 2007 and A. Chérif et al., 2012).

3.4.1 Observer improvement

In order to improve the performances of the observer used, regulator PID in (A. Chérif et al., 2012; A. Chérif et al., 2013) is replaced in this work by a fuzzy- neural regulator as shown in

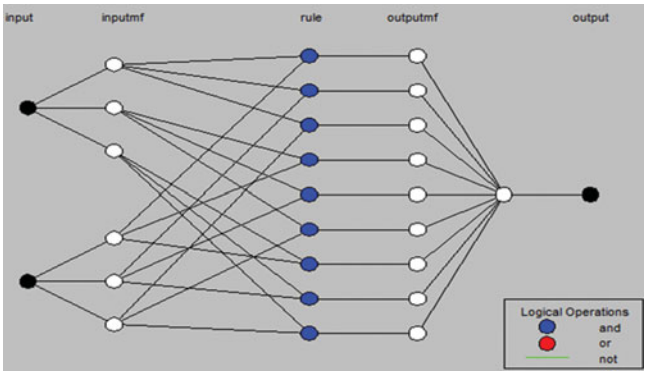

Figure 4. Neuro-fuzzy network architecture.

Figure 3. In Neuro-fuzzy control, neural networks are used to design membership functions of fuzzy systems. They are employed to control the system. This idea was proposed in (Hideyuki Takagi, 1990).

The development cycle of the Neuro-fuzzy model (ANFIS) can be summarized as follows: data-gathering and analysis, choice of neural network architecture and training using the gathered data.

In this work, the training database for the ANFIS model is learned from the simulation model. The chosen Neuro-fuzzy network architecture is given in Figure 4. It comprises two input variables and three membership functions.

The fuzzy controller consists of two inputs: the error (e) which is equal to $\left(V_s - \hat{V}_s\right)$, Figure 3, and the error change (de). The output is defined by the membership functions of Figure 5.

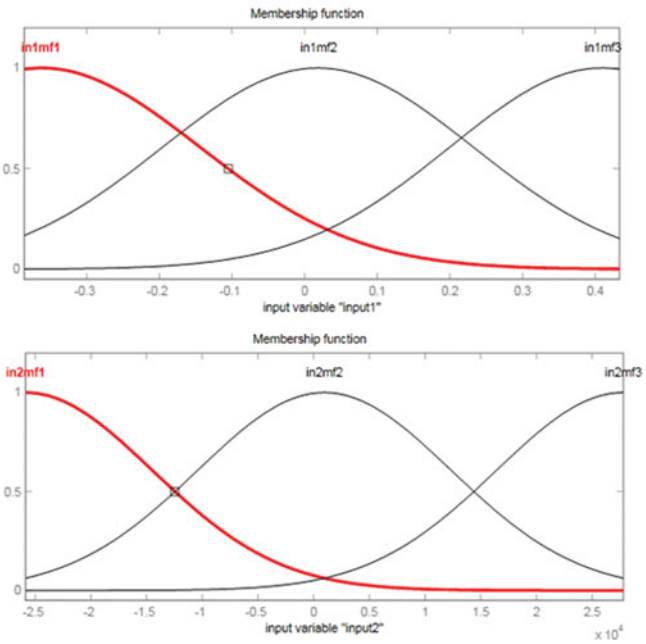

Figure 5. Fuzzy controller membership functions: (down) inputs1 (e) and (top) input2 (de).

Table 1. Coefficients a, b and c.

[a b c] for the nine membership functions		
[127.6	− 3.493e-005	− 2.253]
[132.1	− 1.381e-005	0.1343]
[131.7	− 1.472e-005	0.7989]
[129.4	7.673e-006	0.4491]
[132.1	8.453e-006	− 0.06528]
[132	1.847e-005	− 0.3501]
[93.69	− 0.0008193	− 1.83]
[136.1	− 0.0001929	− 0.4182]
[127.9	− 0.000232	6.853]

Table 2. Characteristics of the clamped plate.

Parameter	Real value
Length	0.6 m
Width	0.4m
Thickness	1 mm
Young modulus	210 GPa
Poisson ratio	0.345
Density	7500 Kg/m3

The controller output is calculated using the following equation:

$$y = a.x_1 + b.x_2 + c,$$

Where y is the output, x_1 is the input1 (e) and x_2 is the input 2 (de) and coefficients a, b and c (for the nine output membership functions) are given in table 1.

4. Simulation results

The simulation, of the smart structure, has been performed under the Matlab/Simulink^{TM} environment.

4.1 Smart structure definition

The smart structure used in the simulation is a steel plate fixed on the four sides and equipped with four piezoelectric inserts PZT P188. (Figure 6).

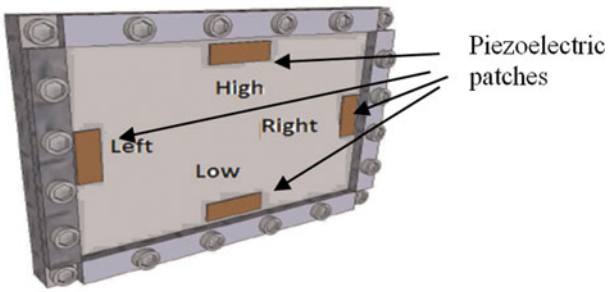

Figure 6. Protective panel structure used for the simulation. The plate is clamped on the four sides. The size of the piezoelectric elements is 12× 4 cm2 and 600 μm thick.

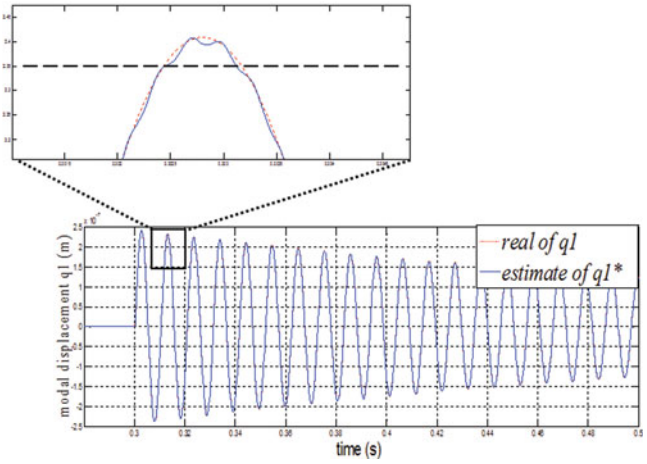

Figure 7. Real (red) and estimated (blue) modal coordinates for mode 1 using the LQG+PID method without control (with zoomof the framed area).

The dimensions and the physical properties of the plate are given in tables 2 and 3 (S. Harari et al., 2009). The structure has been identified according to the model described previously. The procedure of measurement and identification of the parameters is detailed in (S. Harari et al., 2009).

4.2 Observer performances

In this section, the performances of the proposed observer will be compared with those of the observer based on PID regulator. The two observers will be tested in both open-loop and closed-loop cases.

4.2.1 Open-loop case

The structure model presented in § 4.1 has been simulated by using three patches as sensors to feed the observer, and the other patche was left in open circuit; therefore, in this section the system is without vibrations control. The excitation is a pulse square force of $50\mu s$ with a normalized amplitude.

In order to compare the two various configurations of observers, the real and the estimate of the modal coordinates q_1 and q_4 (first and forth modal coordinates) are compared.

Figures 7 and 9 illustrate the comparison of modes 1 and 4 respectively using the PID-based observer design. Otherwise, Figures 8 and 10 show the same comparison in the case of

Table 3. Characteristics of PZT P189 piezoelectric patches.

Property	Symbol	Real value
Density	ρ	7650 Kg.m^3
Compliances CC	s^E_{11}	10.66×10^{-12} Pa^{-1}
	s^E_{22}	-3.34×10^{-12} Pa^{-1}
	s^E_{33}	-4.52×10^{-12} Pa^{-1}
	s^E_{44}	13.25×10^{-12} Pa^{-1}
Permittivity	ε^1_{33}	10.17 nF.m^{-1}
Piezoelectric coefficient	d_{11}	-108 pC.N^{-1}

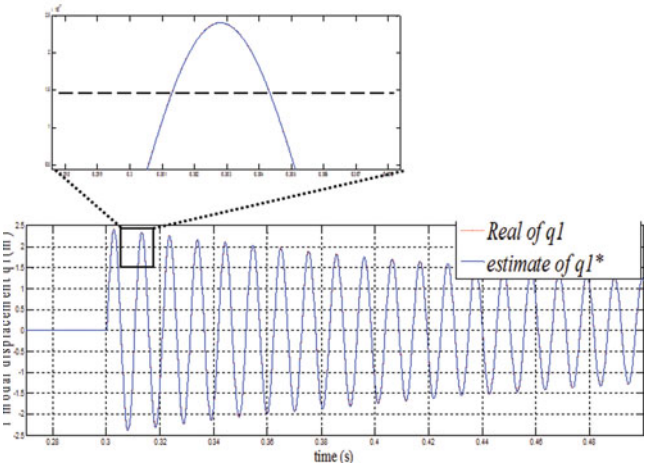

Figure 8. Real (red) and estimated (blue) modal coordinates for mode 1 using the LQG+NF method without control (with zoom of the framed area).

the NF-based one. All the figures are associated with a zoom of a part of response arbiterary chosen whereas the modal displacement seems to be superposed.

We can see clearly in the figures 7 and 9 that the crests of the estimate modal displacement present bumps where few points only overlap with the real modal coordinates (q_1 and q_4). Otherwise, the crests of the estimate and real modal coordinates are superposed for q_1 (see zoom Figure 8) and overlap on several points for q_4 (see zoom Figure10). We see well so that the LQG+NF architecture, in open-loop, provides a quick and a best convergence in comparison with the LQG+PID architecture.

4.2.2 Closed-loop case

a) ***Pulse square excitation.*** Since, the modal observer acts rather in the dynamic cases as the nonlinearity affects the system responses. We study, here the case of the closed loop. In

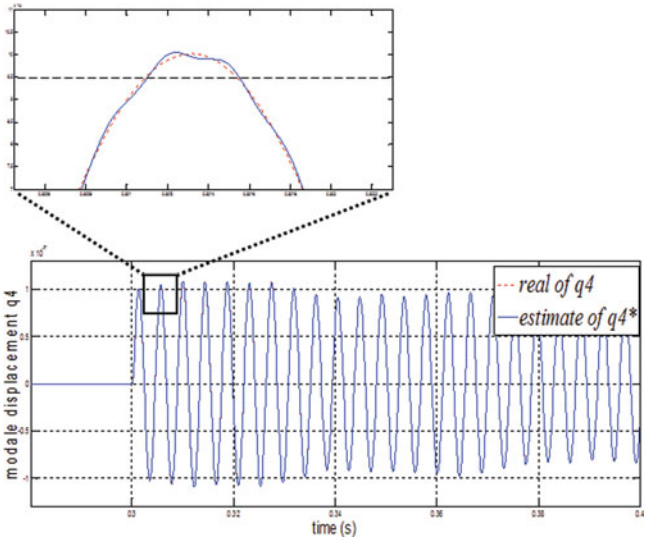

Figure 9. Real (red) and estimated (blue) modal coordinates for mode 4 using the LQG+PID method without control (with zoom of the framed area).

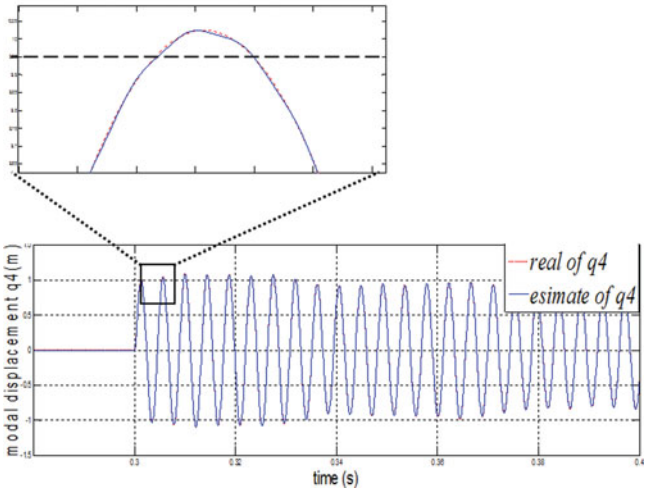

Figure 10. Real (red) and estimated (blue) modal coordinates for mode 4 using the LQG+NF method without control (with zoom of the framed area).

order to analysis the performances of the improved observer, the same simulations than that previously were performed. The SSDI-Max method was used as control technique.

Figures 11, 13 (see zoom of the crests) show that the crests form of the real and estimated modal coordinates (q_1 and q_4 respectively) were different.

The oscillations on the estimated coordinates (see crests) were more damped. The observer LQG+PID approaches so little the estimated response to the real response.

In the figures 12 (for q_1) and 14 (for q_4), one can see already that the improved observer (LQG+NF) functionning in closed-loop reduces the observed oscillations in the figures 11 and 13 (see zooms). The zoom of the considered crests were different point of view form and oscillations of the estimated modal coordinates. Otherwise, the estimated and the real modal coordinates were superposed for the two modes q_1 and q_4. We can say that the improved

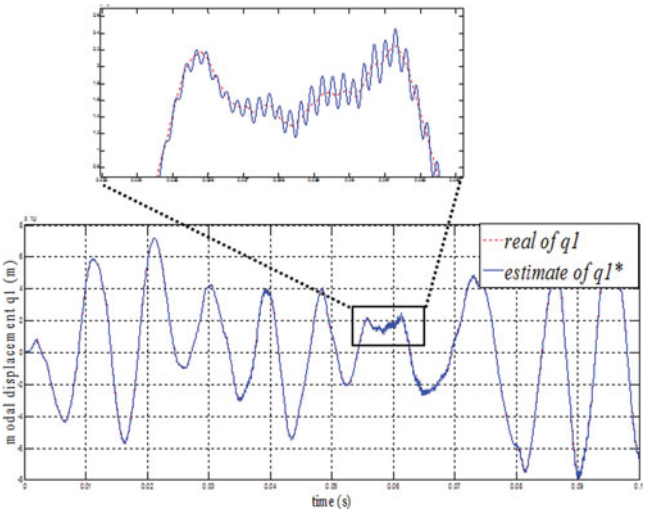

Figure 11. Real (red) and estimated (blue) modal coordinates for mode 1 using the LQG+PID method under control (with zoom of the framed area).

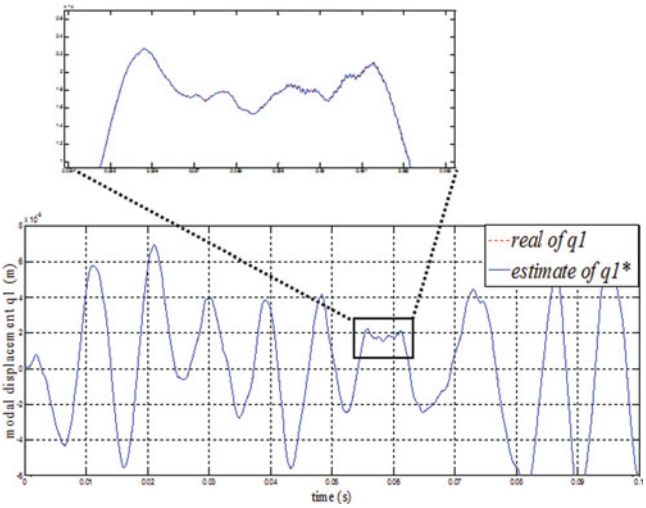

Figure 12. Real (red) and estimated (blue) modal coordinates for mode 1 using the LQG+NF method under control (with zoom of the framed area).

observer (LQG+NF) in closed-loop, using SSDI-Max as control technique, well approached the estimated to the real modal coordinates.

b) ***White noise excitation.*** The closed-loop using the improved observer, in the previous section, gave a good result. This one has been tested on the responses of displacement and the voltage of the transducer. Simulations were made using a white noise excitation and the control was targeted on the modal displacement 1.

Figure 15 illustrates the comparison between the two responses of displacement using the two observers, and the figure 16 represents the two transducer1 voltages. In the figure 15 we can see well that the new observer attenuates the modal displacement. The effect of the Neuro-Fuzzy observer on the voltage of the piezoelectric transducer is shown in Figure 16. The

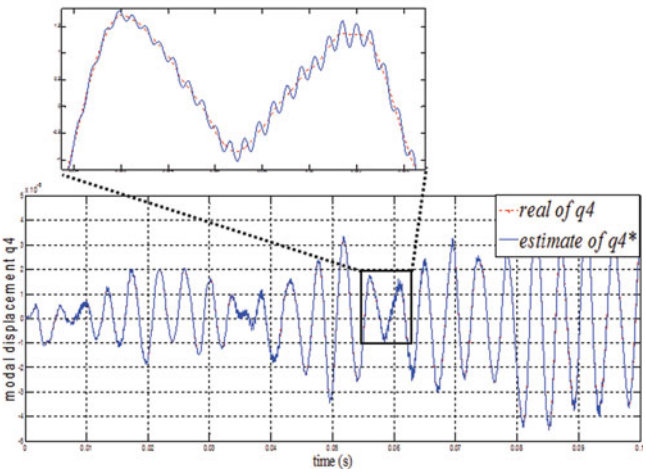

Figure 13. Real (red) and estimated (blue) modal coordinates for mode 4 using the LQG+PID method under control (with zoom of the framed area).

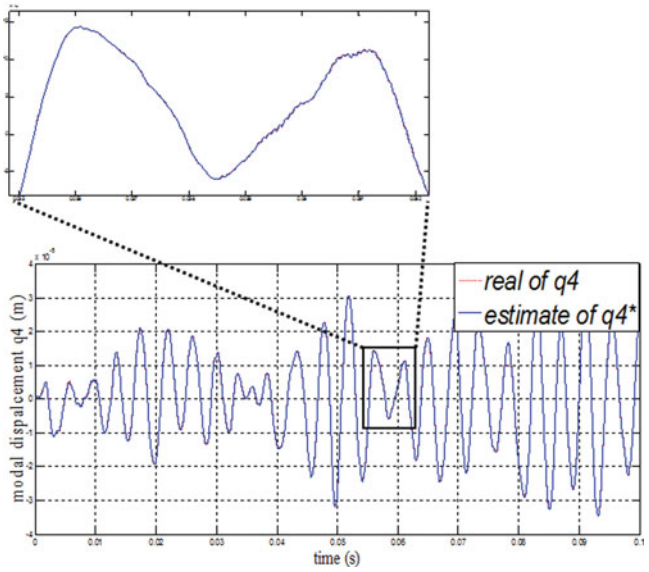

Figure 14. Real (red) and estimated (blue) modal coordinates for mode 4 using the LQG+NF method under control (with zoom of the framed area).

voltage of this later is increased in comparison with the result obtained with the LQG+PID observer (see Figure16).

In this latter, the many inversions of voltage having too small amplitudes due to the harmonics, on the displacement image given by, the PID based observer performances seems to be limited to maximize the transducer voltage and drives to a weak damping. It is in agreement with literature (S. Harari et al., 2009; A. Chérif et al., 2012).

When the NF based observer was used, the precise image leads to precise trigger instants which increase significantly the actuator voltage and as a result maximize the damping.

4.3 SSDI and SSDI-Max modal

In this part, we compared the two controls SSDI and SSDI-Max using the proposed observer. They were tested with three types of broadband excitation: pulse, sum of sinusoids and white noise. In these simulations, only one piezoelectric element is used as actuator. The three others are used as sensors to feed the observer. The strategy consists in targeting the first mode.

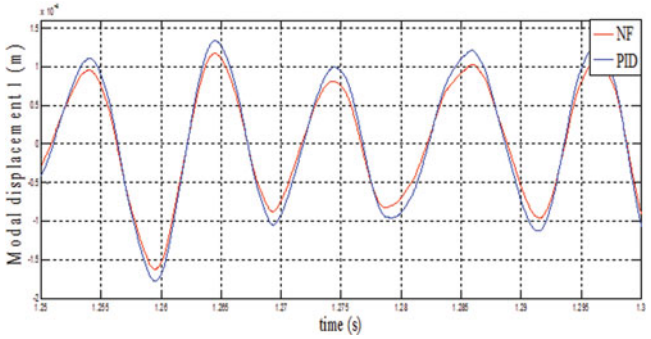

Figure 15. Modal coordinates for mode 1 using the LQG+NF obsever (red) and LQG+PID obsever (blue).

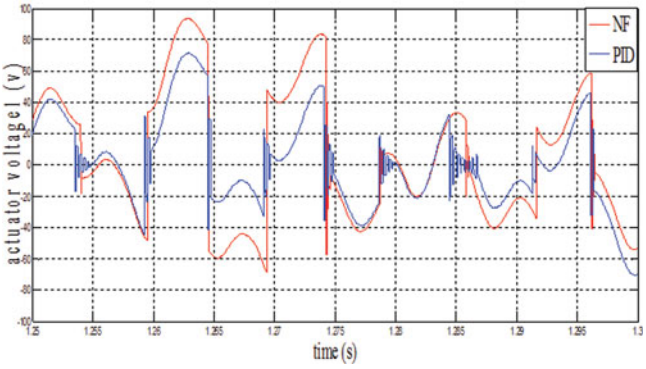

Figure 16. Voltage in the transducer 1 using the LQG+NF obsever (red) and LQG+PID obsever (blue).

a) ***Pulse excitation.*** The excitation is a pulse square of 50 μs and normalized amplitude. Figure 17 shows the modal displacement (mode 1) where the LQG+NFobserver has been used in order to compare its performances under SSDI-Max and SSDI control.

We can see that from the time 0.43 s, the displacement was totally damped under the SSDI-Max control. However, a partial damping was observed on all the duration of the simulation under SSDI control. The total damping was obtained rather beyond of the time 0.52 s. However, the transducer voltage increases under the SSDI-Max control in comparison with the SSDI control (Figure 18). However, the modal displacement was zero whereas the transducer was disconnected (without control).

b) ***Sinusoidal and white noise excitation.*** The improved observer and the SSDI-Max control have been tested by using the sum of four sinusoidal signals. The frequencies of the four modes were electromechanically coupled (T. Richard, 2007).

The figures 19 and 20 present respectively the displacements and the transducer voltages. We see well that the SSDI-Max control gives a displacement more damped in comparison with SSDI control. The same test has been made by using the white noise excitation. The results were similar to that obtained previously (Figure 21 and Figure 22). In all the cases the displacements decrease and the transducer voltages increase (zero without control) as previously.

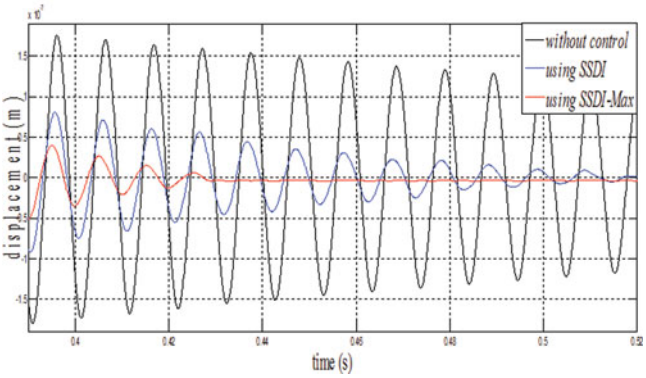

Figure 17. Modal displacement 1 using the LQG+NF obsever with SSDI-Max (red), SSDI (blue) and without control (black) in the pulse case.

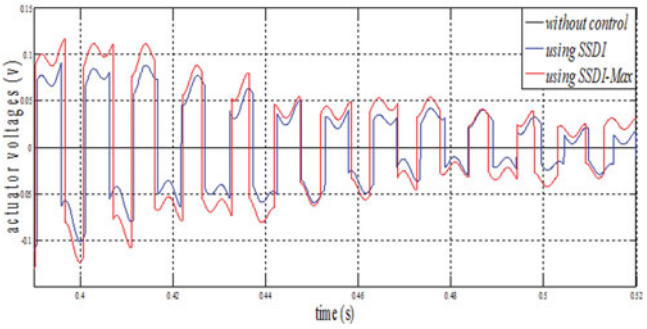

Figure 18. Transducer voltage using the LQG+NF obsever with SSDI-Max (red), SSDI (blue) and without control (black) in the pulse case.

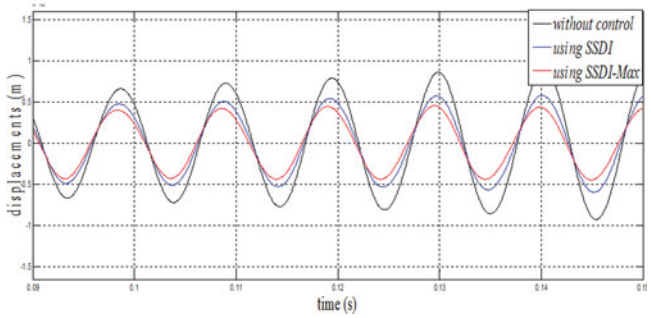

Figure 19. Modal displacement 1using the LQG+NFobsever with SSDI-Max (red), SSDI (blue) and without control (black) in the sinusoidal case.

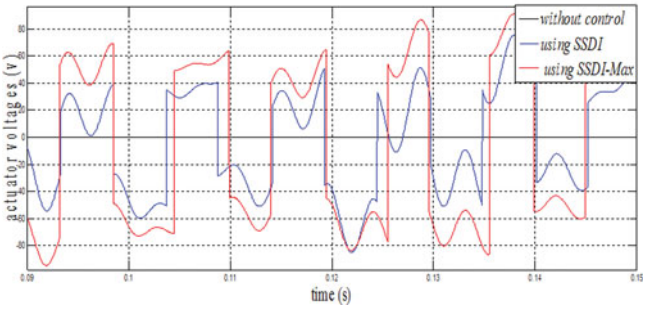

Figure 20. Transducer voltage using the LQG+NF obsever with SSDI-Max (red), SSDI (blue) and without control (black) in the sinusoidal case.

As it is known, the damping performances are strongly dependent on the generated piezoelectric actuator voltage (V_a), figures 18, 20 and 22 for the three excitation types. These one illustrate so the considerable increase in this voltage when the SSDI-Max strategy was used instead the SSDI control. Moreover, it is clearly visible in figures 17, 19 and 21 that a strong improvement of damping was observed by using SSDI-Max method.

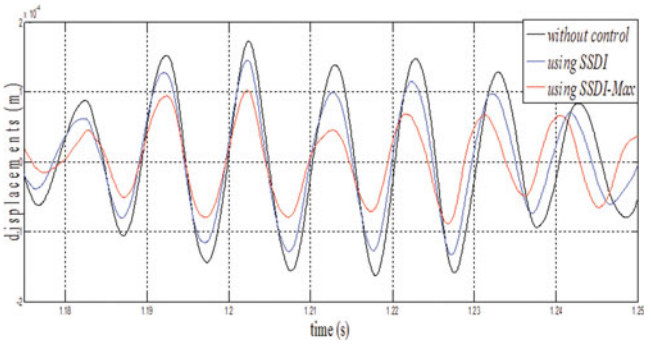

Figure 21. Modal displacement 1using the LQG+NFobsever with SSDI-Max (red), SSDI (blue) and without control (black) in the white noise case.

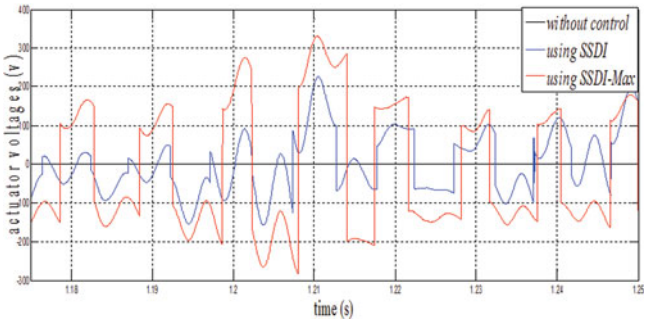

Figure 22. Transducer voltage using the LQG+NF obsever with SSDI-Max (red), SSDI (blue) and without control (black) in the white noise case.

5. Conclusion

In this paper, the performances of modal SSDI-Max strategy based on enhanced LQG+Neuro-Fuzzy observer are presented and compared with that one based on LQG+PID observer. The particularity of this work was the significant improvement of the modal coordinate's image given by the observer whereas the damping performances are strongly related. In the same time, a remarkable maximization of the self-generated voltage amplitude was obtained by a self-definition of the voltage inversion instants according to the chosen targeted mode.

The simulation results obtained using the improved observer showed well that the semi-active methods, based on the modal strategy, are practical solutions suited to the real vibration damping especially in the case of the broadband frequencies. Simulations are performed on a model representative of a clamped plate and the results are given in three multimodal cases whereas these methods allow targeting any undesirable vibration mode. Finally, it was shown that the proposed observer offers better performances in both open and closed loop tests and in all the cases of excitation.

References

[1] Badel, A., Sebald, G., Guyomar, D., Lallart, M., Lefeuvre, E., Richard, C., & Qiu, J. (2006). *Journal of the Acoustical Society of America*, *119*(5): 2815–2825.

[2] Chérif, A., Richard, C., Guyomar, D., Belkhiat, S., Meddad, M., Eddiai, A., & Hajjajid, A. (2013). *Journal of Optoelectronics and Advanced Materials*, *15*: 438–446.

[3] Chérif, A., Richard, C., Guyomar, D., Belkhiat, S., & Meddad, M. (2012). *Journal of Intelligent Material Systems and Structures*, *16*: 1–16.
[4] Chérif, A., Meddad, M., Belkhiat, S., Richard, C., Guyomar, D., Eddiai, A., & Hajjaji, A. (2013). *Optical and Quantum Electronics*, DOI 10.1007/s11082-013-9712-2.
[5] Chérif, A. (2012). Optimisation du transformateur piézoélectrique. Application: contrôle semi-passive des vibrations, PhD thesis in Ferhat Abbas University – Sétif UFAS (Algeria).
[6] Fleming, A. J., & Moheimani, S. O. R. (2003). *IOP Smart Materials and Structures*, *12*: 36–48.
[7] Mokrani, B., Rodrigues, G., Ioan, B., Bastaits, R., & Preumont, A. (2011). *Journal of Intelligent Material Systems and Structures*, *23*(18): 2065–2075.
[8] Park, C. H. & Inman, D. J. (2003). *Shock and Vibration*, *10* (2): 127–133.
[9] Richard, C., Guyomar, D., Audigier, D., & Ching, G. (1999). Semi-passive Damping Using Continuous Switching of Piezoelectric Devices, in *Proceedings of SPIE Conference on Passive Damping and Isolation*, Newport Beach, CA, *3672*:104-111.
[10] Richard, C., Guyomar, D., Audigier, D., & Bassaler, H. (2000). Enhanced semi-passive damping using continuous switching of a piezoelectric devices on an inductor in *Proc. SPIE Smart Structures and Materials, Damping and Isolation,* (Newport Beach, CA), *3989*: 288–299.
[11] Guyomar, D., Richard, T., & Richard, C. (2008). *Journal of Intelligent Material Systems and Structures*, *19*: 791–803.
[12] Luenberger, D. (1971). *Automatic Control, IEEE Transactions*, *16*(6): 596–602.
[13] Babesse, E., Chérif, A., Belkhiat, S., & Meddad, M. (2013). *Proceedings Engineering & Technology – June Sousse Tunisia*, *2*: 84–89.
[14] Takagi, H. (1990). Fusion technology of fuzzy theory and neural networks - Survey and future directions, International Conference on Fuzzy Logic & Neural Networks (IIZUKA-90), 1: 13-26.
[15] Lallart, M. (2010). Vibration Control, Sciyo, Croatia.
[16] Hagood, N. W., & Von Flotow, A. (1991). *Journal of Sound and Vibration*, *146*(2): 243–268.
[17] Forward, R. L. (1979). *Applied Optics*, *18*(5): 690–697.
[18] Harari, S., Richard, C., & Gaudiller, L. (2009). *Journal of Intelligent Material Systems and Structures*, *20*: 1603–1613 .
[19] Harari, S., Richard, C., & Gaudiller, L. (2009). Semi-active control of a targeted mode of smart structures submitted to multimodal excitation, in 9th International Conference on Motion and Vibration Control, 113-122.
[20] Harari, S., Richard, C., & Gaudiller, L., (2009). *Journal of Intelligent Material Systems and Structures*, *20*: 1603–1613.
[21] Harari, S., Richard, C., & Gaudiller, L. (2009). *Motion and Vibration Control: Selected Papers from MOVIC 2008*, *1*: 113–122.
[22] Richard, T. (2007). Diminution du coefficient de transmission acoustique d'une paroi à l'aide d'amortisseurs piézoélectriques semi-passifs, PhD thesis in INSA Lyon French.